Robotica (2026), **44**, pp. 2234–2246
doi:10.1017/S0263574726103907

CAMBRIDGE UNIVERSITY PRESS

RESEARCH ARTICLE

Soft dexterous hand with enhanced grasping performance enabled by rigid-flexible structure and visual perception

Ruiqi Yin†, Chuanwang Liu†, Zhenhao Sun, Shihao Sun, Shuhai Liu and Huaping Xiao

China University of Petroleum Beijing, China
Corresponding author: Huaping Xiao; Email: hxiao@cup.edu.cn

Received: 30 April 2026 UTC; **Revised:** 16 July 2026 UTC; **Accepted:** 7 August 2026 UTC;
First published online: 21 September 2026 UTC

Keywords: soft dexterous hand; rigid-flexible structure; visual perception; autonomous grasping; soft robots

Abstract

Soft robotic hands face trade-offs between flexibility and load capacity, with rigid-palm designs limiting grasping conformity and fully soft structures struggling under payloads. Existing pneumatic systems suffer from tubing interference and poor sealing. This study presents a bioinspired modular hand combining rigid supports and soft actuators to enhance stability and payload (2 N fingertip force at 300 kPa; 1.97 kg maximum grasping payload). A biomimetic thenar joint and rigid linkages optimize thumb-mediated grasping, while built-in pneumatic channels eliminate external tubing, improving reliability. Integrated with RGB-D vision and robotic arm coordination, the system achieved autonomous grasping with 87.22% and 83.33% success rates in single- and multi-object tasks, respectively. This hybrid rigid-flexible approach advances dexterous robotic manipulation by synergizing structural adaptability, modular maintenance, and intelligent perception for practical robotic applications.

1. Introduction

Soft dexterous hands, characterized by their compliance, adaptability, and biomimetic design, mark a transformative advancement in robotics. Unlike traditional rigid manipulators, these systems excel in handling fragile objects, navigating unstructured environments, and enabling safe human–robot interaction. By mimicking the biomechanics of human hands, they bridge the gap between mechanical efficiency and biological elegance, making them indispensable in healthcare, industry, and beyond [27, 30].

The primary advantage of soft dexterous hands lies in their intrinsic safety and adaptability [4]. Utilizing materials such as silicone and thermoplastic polyurethane (TPU), they replicate the compliance of human tissue, minimizing risks in human-centric applications like medical rehabilitation and service robotics [20, 22, 26]. Their passive shape conformity allows stable grasping of irregular objects without complex control systems, a critical feature for industrial automation and delicate tasks [11, 25]. In healthcare, soft robotic gloves restore grip functionality for patients with motor impairments, while sensorized tools like the STIFF-FLOP system enhance precision in minimally invasive surgery [6, 13, 16]. Furthermore, biological inspiration-such as tendon-driven actuation and multi-joint coordination-enables dexterity comparable to human hands, fostering applications requiring nuanced manipulation [12].

MIT's soft robotic hand pioneered adaptive grasping [7], while the Pisa/IIT SoftHand introduced "adaptive synergies," achieving 19 joints with a single actuator [14]. Advances in materials and fabrication, including 3D printing and novel elastomers, enable precise actuator designs, enhancing functionality [32, 33]. Breakthroughs in control algorithms, such as reinforcement learning and capacitive tactile feedback, improve adaptability in uncertain environments [5, 26]. Recent innovations, like

† These authors are contributed equally to this work.

© The Author(s), 2026. Published by Cambridge University Press.

https://doi.org/10.1017/S0263574726103907 Published online by Cambridge University Press

the pneumatically driven RBO Hand 3 and vision-based tactile sensor, demonstrate modularity and bioinspired kinematics, expanding industrial and medical applications [31].

Despite progress, challenges remain. Existing designs of soft dexterous hands face limitations in flexibility, structural support, gripping force, and intelligence [19]. Current popular configurations of soft hand include rigid palm incorporated with soft fingers and fully soft hand. While rigid palms enhance load-bearing capacity, their inability to deform causes inadequate surface conformation, leading to reduced contact area and suboptimal force distribution [9]. This structural rigidity additionally compromises manual dexterity. During the grasping of irregular objects, restricted joint bending angles prevent the fingers from conforming to object surfaces as effectively as human hands [21]. Conversely, fully soft robotic hands demonstrate significantly improved flexibility but suffer from inherent limitations due to the low intrinsic stiffness of compliant materials, which severely restricts their payload capacity [1]. For example, soft fingers exhibit spontaneous gravitational deformation under self-weight loading, particularly pronounced in extended configurations.

Furthermore, contemporary pneumatic soft robotic hands typically employ tubing connections with insertion-type interfaces and adhesive-based sealing at component junctions. External pneumatic lines induce interference during soft actuator deformation, progressively degrading kinematic accuracy. The insertion mechanism induces structural compromise in base materials through penetration damage, significantly impairing mechanical integrity. Simultaneously, adhesive-bonded seals demonstrate inadequate hermetic performance, manifesting as persistent gas leakage during pressurization cycles – a critical limitation in sustained pneumatic actuation. An additional concern is that research on soft dexterous hands remains focused on structural improvements, lacking advanced visual-tactile perception for adaptive grasping in complex environments [10, 23].

In summary, existing dexterous hands face challenges in balancing material compliance with grasping load capacity, along with limitations imposed by external or inserted tubing, which constrain further development. To address these challenges, this study proposes a modular soft hand with a hybrid design integrating soft and rigid components. Novel built-in tubeless pneumatic channels were constructed to enhance system compactness, load capacity, and service life. The main contributions of this study are as follows:

1. The dexterous hand features a modular architecture with standardized interfaces to improve component replaceability, while built-in pneumatic channels enable integrated fabrication and resolve common sealing issues.
2. A bioinspired rigid-flexible hand utilizes soft actuators and rigid supports to boost load-bearing performance. A thenar-inspired thumb joint further enables dexterous precision grasping and high payload capacity (2 N fingertip force, 1.97 kg grasping payload).
3. An RGB-D vision module is integrated to adaptively deploy object recognition and grasping strategies, assisting the soft hand in autonomous multi-object grasping.

2. Design and fabrication of the soft hand

2.1. Design of soft dexterous hand

This study proposed a new type of rigid-flexible coupled modular soft anthropomorphic dexterous hand. This hand, which has a total of 12 degrees of freedom, is composed of three major modules, namely the soft actuator module, the connection module, and the fixation module (Figure 1(a) and (b)).

The soft actuator module consists of finger modules (index finger, middle finger, ring finger, little finger, and thumb), a palm module, and a thenar module. They are all constructed with monolithic tubeless soft bellows structures. In particular, each finger actuator is designed with two independently actuatable pneumatic chambers (Top unit and Base unit), whose built-in pneumatic channels are monolithically molded with the finger body (Figure 1(c)). On the palmar side of the fingers, transverse ridges and herringbone indentations are designed to enhance grasping compliance. The palm module is composed

https://doi.org/10.1017/S0263574726103907 Published online by Cambridge University Press

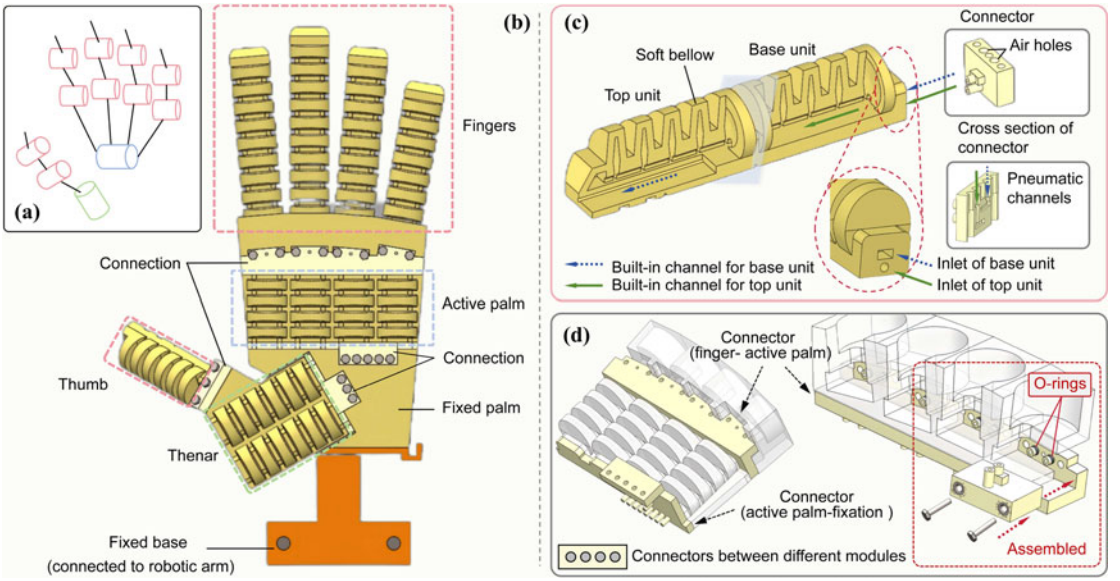


Figure 1. *Structure of the proposed dexterous hand. (a) The soft hand features 12 independent joint axes. (b) Front view of the dexterous hand. (c) Cross-sectional view of the index finger and the connector, which illustrates the matching built-in pneumatic channels. (d) Structure of the connection module, which demonstrates the assembly of the thumb to the palm via the connector.*

of four soft actuators connected in parallel and is responsible for the small angle bending of the palm, which simulates the flexion of the metacarpophalangeal joints. The thenar module contains two parallel soft actuators and provides the thenar bending capability, which provides a foundation for the opposition of the thumb.

The connection module indicates connectors between two actuator modules or an actuator module and a fixed module in Figure 1(d). These connectors feature built-in multiple pneumatic channels, sealing structures, and threaded connections, which enable airtight gas transmission between actuator modules. The fixation module consists of a single fixed palm and a fixed base, which provides support for the entire hand and attaches the palm to the robotic arm. Both the connection and fixation modules are made of tough resin material. More detailed structures of finger actuators and built-in channels are available in supplementary materials (section S1 and Figure S1). How the structural parameters were determined is depicted in section S2.

The hybrid rigid-flexible architecture establishes a mechanical foundation for intricate manipulation by integrating localized stiffening zones, while preserving adaptive deformation capabilities in response to external stimuli. The modular design facilitates the disassembly, replacement, and installation of each component. The built-in tubeless pneumatic channels enable each actuator independent multi-DOFs deformation while eliminating constraints on deformation caused by external tubing and significantly extending the service life.

2.2. Fabrication

The soft dexterous hand proposed in this study was fabricated via casting and lost-wax methodologies. Detailed fabrication procedure is illustrated in Figure 2. First, the pre-fabricated wax core was combined with individually 3D-printed molds to form a complete mold assembly. Subsequently, components A and B of urethane rubber (ReoFlex60, Smooth On) were thoroughly mixed and degassed, injected into the assembled mold, and cooled at room temperature. Thereafter, the cured actuators were carefully removed from the mold. The formed actuators were placed in a constant-temperature drying

https://doi.org/10.1017/S0263574726103907 Published online by Cambridge University Press

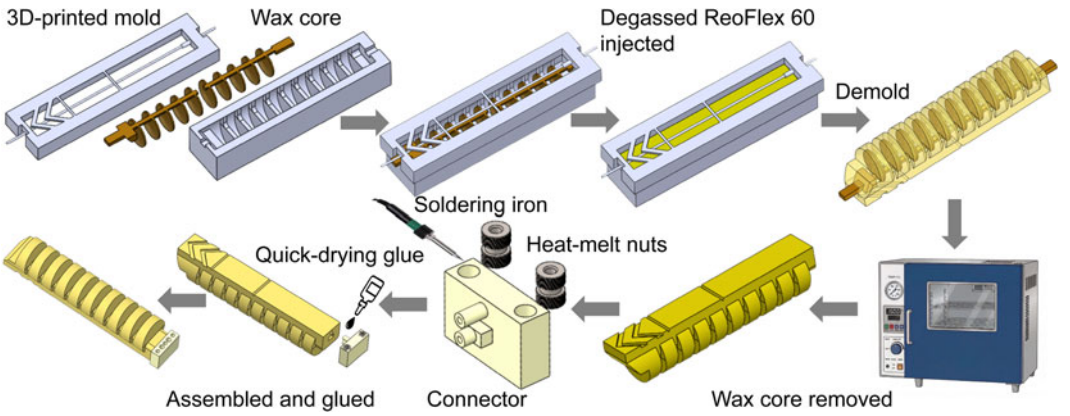


Figure 2. *Manufacturing process of the soft actuator.*

oven set at 120°C for 20 min to ensure complete melting and outflow of the internal wax core, yielding the actuator.

Following the casting of driving modules, the connectors were fabricated using photocuring 3D printing technology with tough resin material. Heat-melt nuts were embedded into the connector. JL-469 type TPU quick-drying glue was then applied to bond the finger module and the connector. Active actuators and fixed parts were assembled using bolts to build the soft hand illustrated in Figure 1.

The implementation of the lost-wax method ensured structural integrity of pneumatic actuators, addressing the issue whereby traditional pneumatic actuators suffer from bond failure and air leakage under high-pressure conditions. Additionally, the integration of built-in pneumatic channels sealed with O-rings at joint interfaces mitigated the common problem of external air leakage in conventional designs, ensuring functional reliability.

3. Characterization of the soft actuator module

3.1. Bending performance

This section investigates the bending performance of the monolithic tubeless soft bellows. Driving pressure incrementally increased from 0 kPa to 300 kPa (limited to 250 kPa for the palm actuator due to its thinner walls). For precise tracking of displacement trajectories under varying pressures, 4 mm-diameter fluorescent markers were sequentially attached along the multi-joint actuator surface. A camera was used to record the spatial displacement of these markers in a dark-field environment, enabling acquisition of kinematic data for all joint segments (fingers, thumb, thenar, and palm regions) as shown in Figure 3.

Figure 3(a) demonstrates the fluorescent bending trajectory of the middle finger. When the pressure is 300 kPa, the top unit reaches 78°, while the base unit achieves 97°. When both units are pressurized, the middle finger displays a 175° bending. Figure 3(d) and (c) present bending trajectories of the little finger and index finger.

The thumb's fluorescent trajectories from multiple perspectives are displayed in Figure 3(b). Front-view measurements show thumb bending angles of 72° (top unit), 74° (base unit), and 125° (both units). This non-superpositional behavior stems from the spatial offset between the thumb's installation plane and the thenar bending plane. The measured maximum bending angles for the thenar and the palm are 56° (Figure 3(e)) and 94° (Figure 3(f)), respectively, demonstrating the favorable bending performance of the soft actuators.

3.2. Output thrusting force

To investigate the output force capacities of the deformable joints in the soft hand, an output force testing platform was constructed (Figure 4(a)–(c)). The driving pressure was incrementally increased

https://doi.org/10.1017/S0263574726103907 Published online by Cambridge University Press

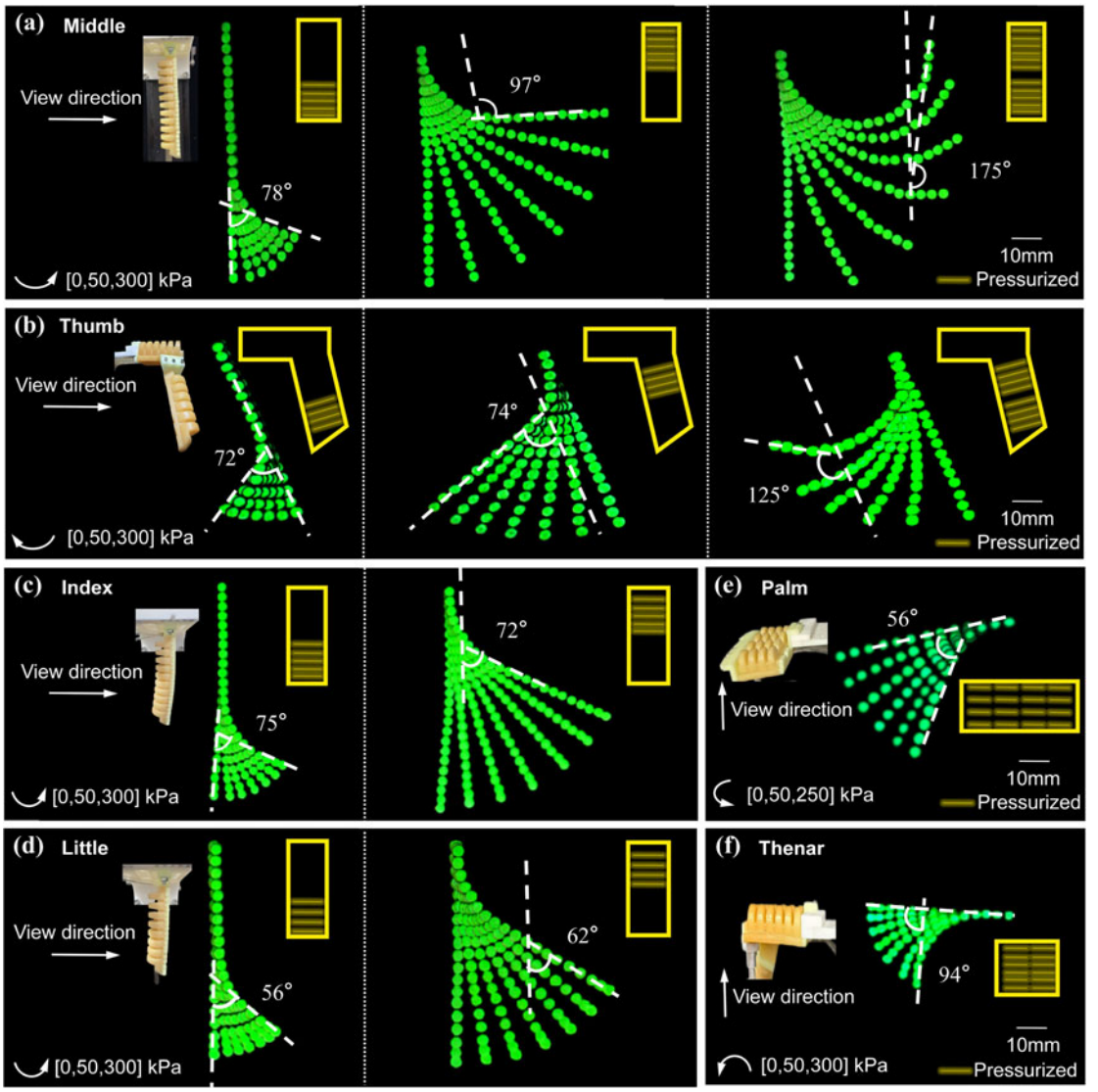


Figure 3. *Fluorescent bending trajectory of the actuators with different driving units being pressurized, (a) middle finger, (b) thumb, (c) index finger, (d) little finger, (e) palm, and (f) thenar.*

from 0 kPa to 300 kPa (limited to 250 kPa for the palm actuator). Since the structural similarity between the thumb and little finger, as well as between the index and ring fingers, only three fingers were tested.

Figure 4(d)–(f) illustrates the results of the average output thrust for the index finger, middle finger, and thumb. The experimental data reveal a near-linear correlation between fingertip output force and base unit pressure under constant top unit pressure across all tested fingers. Conversely, when maintaining constant base unit pressure, the relationship between fingertip output force and top unit pressure demonstrates nonlinear behavior. At low base unit pressures (0–50 kPa), a positive correlation exists between fingertip output force and top unit pressure. However, under elevated base pressures (100–300 kPa), the output force initially decreases before rising with the increasing top pressure. This phenomenon arises from significant fingertip reverse bending under high base unit pressure with unpressurized top units. This reverse bending occurs due to limited material rigidity and dynamometer displacement constraints. Consequently, pressurizing the top unit must first counteract this deflection, which initially

https://doi.org/10.1017/S0263574726103907 Published online by Cambridge University Press

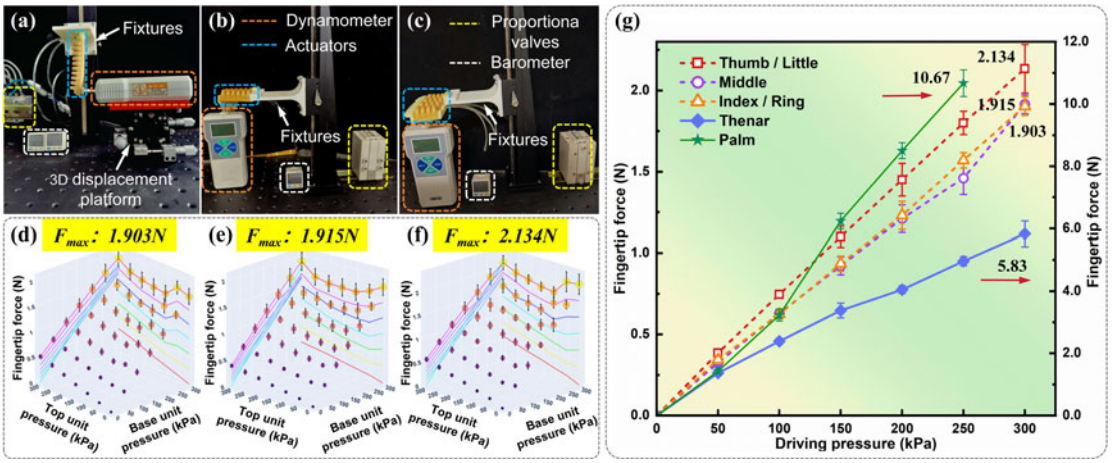


Figure 4. *Thrusting force tests for finger (a), thenar (b), and palm (c). Output force of different fingers, (d) index/ring, (e) middle, and (f) thumb/little. (g) Output force of all actuators.*

reduces the measured force. Progressive top unit pressurization eventually converts reverse bending to forward bending, enabling sustained force enhancement.

Figure 4(g) summarizes the thrust performance of all actuators. Finger actuators achieved maximum fingertip forces of 1.903 N (index/ring), 1.915 N (middle), and 2.134 N (thumb/little) at 300 kPa driving pressure for both units. Under combined pressure conditions (300 kPa top/0 kPa base units), forces measured 1.734 N, 1.814 N, and 2.012 N, respectively. Conversely, 300 kPa base/0 kPa top unit configurations yielded reduced outputs of 0.512 N, 0.39 N, and 0.563 N. These measurements demonstrate non-additive force characteristics during simultaneous top and base unit activation. This behavior is caused by antagonistic bending effects, which diminish the theoretical sum of individual unit contributions.

Comparative analysis reveals superior performance in thenar (5.83 N) and palm (10.67 N) actuators at 300 kPa, substantially exceeding finger actuator outputs. This enhancement is achieved through the adoption of a parallel unit configuration (two units for the thenar and four units for the palm). These results confirm that increasing parallel pneumatic units can effectively amplify the output thrust through force superposition. The experimental data quantitatively validate the critical relationship between parallel unit quantity and resultant actuator performance.

4. Visual perception system

To achieve intelligent grasping based on the soft dexterous hand, this study designs a vision-assisted grasping control system. The hardware platform consists of an Orbbec Astra Pro Plus depth camera, a Dobot CR5 robotic arm, a pneumatic control system, and the soft dexterous hand (Figure 5(a)). The system operates through the coordination of four main modules: visual perception, algorithm control, hand–eye coordination, and robotic arm grasping, achieving a complete closed loop from image acquisition to motion control.

Serving as the perception front-end, the depth camera inputs pre-processed high-quality visual data into the computer. The system adopts YOLOv10n (Nano version) pre-trained on the MS COCO dataset as the foundational object detection model. Rather than redesigning the underlying network, the core of visual perception integrates detection results, depth data, and grasping rules to build an adaptive framework for the soft hand (Figure 5(b)). This strategy evaluates the depth validity of the target regions by combining RGB-D information and filters out unreliable targets that suffer from missing depth or excessive depth noise. Utilizing the target's category, bounding box, and depth data, the algorithm estimates its shape and selects the optimal grasping mode (power, thumb-opposed, or precision pinch).

https://doi.org/10.1017/S0263574726103907 Published online by Cambridge University Press

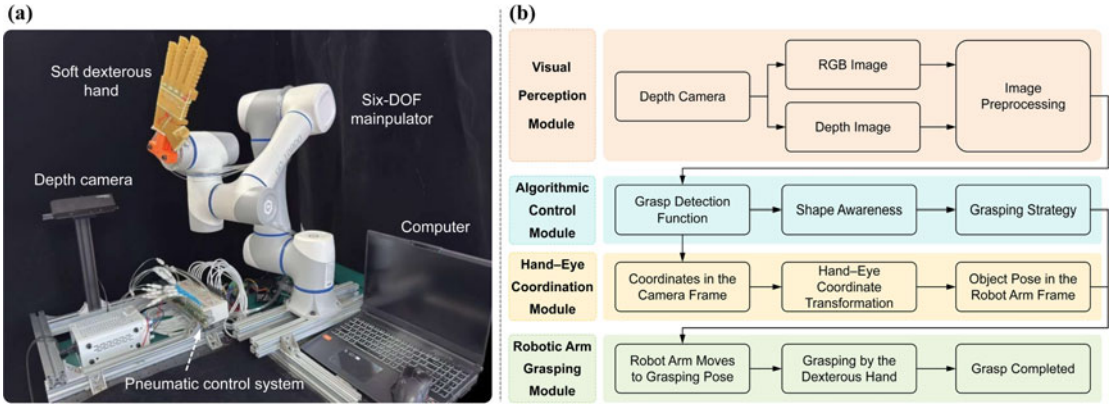


Figure 5. *(a) Vision-guided grasping system platform. (b) Vision-guided Grasping System Framework.*

For multi-object scenarios, the system formulates a graspability scoring function that integrates detection confidence, depth reliability, shape congruence, and adjacent interference to identify the optimal target.

The hand-eye coordination module resolves cross-coordinate positioning using a pre-calibrated transformation matrix. It converts the optimal grasping pose from the camera frame to the robotic arm's base frame, resolving the cross-coordinate positioning issue. The main control computer translates the pose parameters into driving signals in real time, controlling the robotic arm to move to the target position. Meanwhile, the dexterous hand automatically adjusts the gripping air pressure based on the object's shape, driving the fingers to adaptively open and close to complete the grasp. The overall "visual perception-grasping decision" architecture operates stably at approximately 33 FPS, which fully satisfies the real-time response requirements in the experimental scenarios.

5. Performance and applications

To evaluate the performance of the entire anthropomorphic dexterous hand, the maximum grasping force and overall dexterity of the robotic hand were quantified. Additionally, systematic evaluations were conducted on the vision-guided intelligent grasping.

5.1. Performance of the dexterous hand

5.1.1. Maximum grasping capability

Maximum grasping capacity serves as a pivotal performance indicator for soft dexterous hands. This study quantified this parameter under three biomimetic grasping configurations: palm-parallel-to-gravity (PPG) grasping, palm-vertical-to-gravity (PVG) lifting, and palm- parallel-to-gravity (PPG) lifting. The first test protocol involved incrementally filling a plastic bottle with water for mass measurement, while the second employed a basket loaded with standardized lead blocks for precise mass calibration. As demonstrated in Figure 6(b), the soft dexterous hand successfully secured a 630.5 g water bottle in PPG grasping, an 867.5 g basket in PVG lifting, and a 1973 g in PPG lifting.

5.1.2. Grasping performance

This study proposes an adaptive grasping strategy by mimicking the structural characteristics of the human hand. The soft fingers and thenar are designed with a multi-joint configuration, enabling them to automatically conform to the surface of different objects. Supplementary material S4 provides additional details regarding the grasp assessment criteria.

Through material elasticity and joint coordination, the hand executes power, precision, and thumb-opposed grasping without relying on complex sensors (Figure 6(a)). During delicate tasks, it

https://doi.org/10.1017/S0263574726103907 Published online by Cambridge University Press

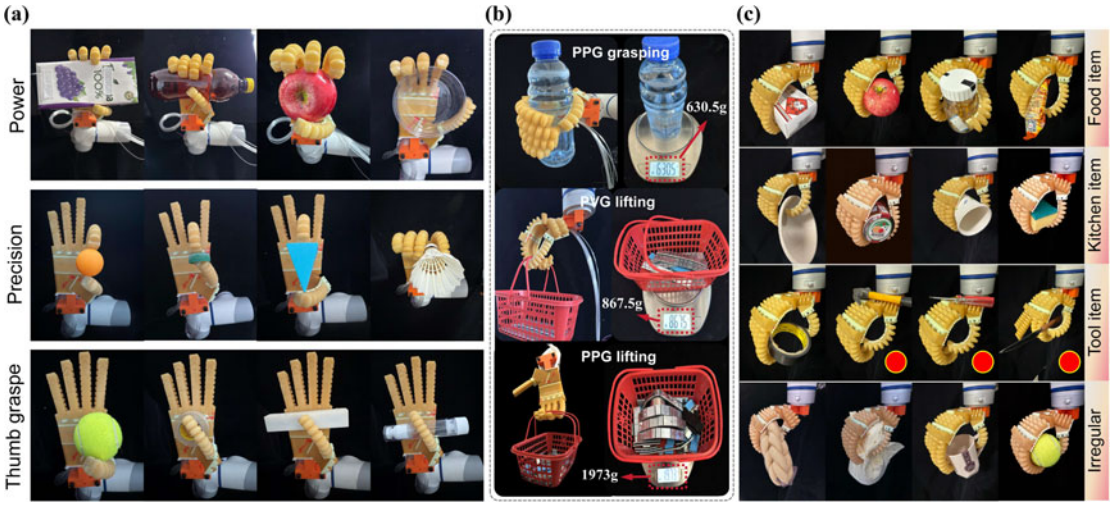


Figure 6. *Performance of the dexterous hand. (a) Demonstration of grasping using different methods. (b) The maximum grasping quality under different postures, including PPG grasping, PVG lifting, and PPG lifting. (c) Various objects of YCB set grasped by the soft hand.*

accurately manipulates small objects via coordinated thumb-index finger movements to realize a precision pinch. In thumb-opposed grasping mode, the soft hand stably retains the object through active deformation of the thenar structure and synergistic motion with the thumb. This design demonstrates robust adaptability across various grasping tasks, highlighting its potential for practical applications in robotics.

The YCB (Yale-CMU-Berkeley) object set [3] was adopted as a standardized benchmark to systematically evaluate the grasping performance of the proposed soft dexterous hand. As illustrated in Figure 6(c), successful and failed grasps (marked in red dot) from the YCB set are presented. Experimental results indicate that the soft hand achieved a high success rate when grasping medium-to-large objects (e.g., food containers, cups, and irregular ornaments). This success is primarily attributed to the multi-joint deformation, which provides conformable support. However, slippage frequently occurred when manipulating slender or miniature tools (e.g., utensils and precision instruments). This limitation stems from two key factors: dimensional constraints and material compliance effects. The soft anthropomorphic hand is slightly larger than a human hand, and its wider inter-finger spacing hinders effective envelopment of narrow objects. The inherent compliance of fully soft structures complicates pressure distribution, thereby reducing stability during the precise grasping of small items.

Comparison of grasping performance of various soft robotic hands is illustrated in Table I. Experimental results confirm that the proposed soft hand achieves a significant enhancement in maximum grasping mass while preserving high bending angles and relatively low weight. This strategy effectively resolves the trade-off between dexterity and load-bearing capacity, demonstrating marked improvements in both functional metrics.

5.1.3. Cyclic endurance

To further verify the reliability of the soft hand, the actuators were subjected to repeated inflation-deflation cycles. In the configuration where the air tube was directly inserted and sealed with glue, the actuator lasted approximately 2,000 cycles. When the air tube was cast into the finger module, the actuator withstood around 10,000 cycles. By contrast, the proposed actuator utilizes integrated tubeless pneumatic channels and O-ring seals at joint interfaces, surviving 20,000 cycles without damage. After 20,000 cycles, the fingertip output force of the soft actuator was retested. At a driving pressure

https://doi.org/10.1017/S0263574726103907 Published online by Cambridge University Press

https://doi.org/10.1017/S0263574726103907 Published online by Cambridge University Press

Table I. *Comparison of grasping performance of different soft robotic hands.*

References	Weight	Materials	Structure type	DOF of single finger	Maximum of the finger	DOF of the palm	Grasping posture	Target object (Shape & size)	Maximum object weight
[18]	165 g	Dragon skin 10, Dragon skin 30	Fully soft	2	0.8 N	2	PVG lift	A basket with blocks	1.27 kg
[12]	406 g	Ecoflex 00-50, Mold star 30, ABS	Rigid palm + soft fingers	3	1.29 N	1	PPG lift	A basket with blocks	1.12 kg
[28]	NA	TPU, particle	Rigid palm + soft fingers	1	NA	2	PPG grasp	3D-printed cylinder	1.45 kg
[17]	350 g	Rigid material	Rigid palm + flexible fingers	1	15 N	0	PPG grasp	Bottled juice	$\geq$ 1.37 kg
[15]	NA	Shore A60 Vero, Agilus	Soft fingers	3	NA	2	helical grasp	Screwdriver	0.654 kg
[2]	100 g	Ecoflex 00-50, PET, TPU	Rigid frame + soft fingers	3	$\leq$ 0.8 N	0	NA	NA	NA
[8]	874 g	Dragon Skin 10, Dragon Skin 20	Rigid palm + flexible fingers	3	NA	1	power grasp	Hammer	0.4 kg
[24]	NA	Dragon Skin 10, PLA	Rigid palm + flexible fingers	3	1.8 N	0	NA	Water bottle	NA
[29]	138 g	Agilus 30 series and Vero series	Rigid palm + soft fingers	2	0.86 N	1	NA	NA	NA
This work	250 g	ReoFlex 60, tough resin	Rigid frame + soft fingers + soft palm	2	2.134 N	1	PPG lift	A basket with blocks	1.97 kg

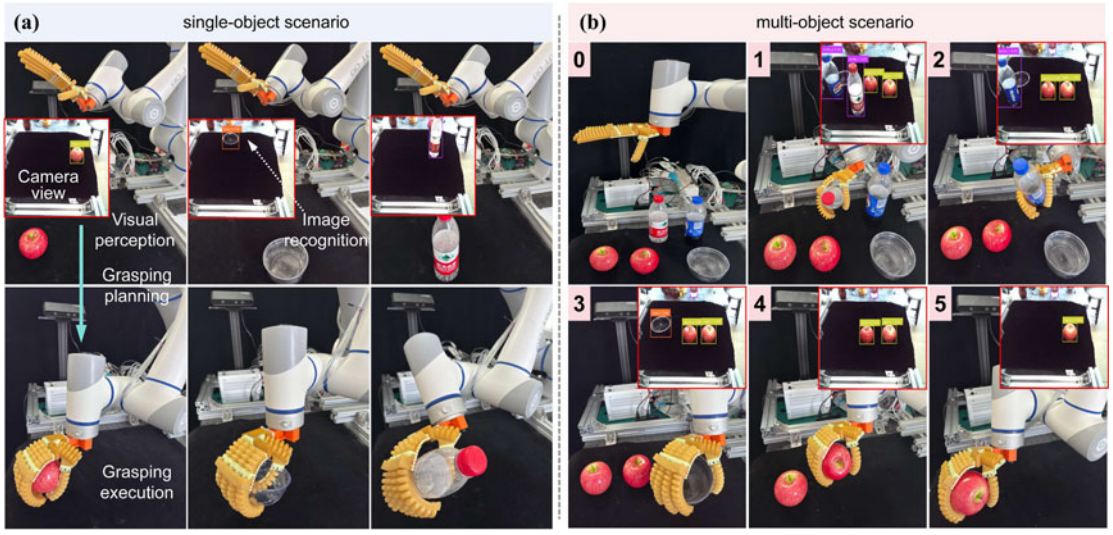


Figure 7. *Visual perception enabled active grasping. (a) Grasping task in single-object scenario. (b) Grasping five items in multi-object scenario (number in each figure indicates number of items removed).*

of 300 kPa, the maximum fingertip forces were 1.897 N (index/ring), compared with 1.903 N before cycling, representing a decrease of 0.315%. A pressure retention test was subsequently conducted on the cycled actuator. When inflated to 300 kPa and held for 60 s, the pressure drop was only 3.2%, demonstrating that high-frequency cycling did not compromise the system's airtightness. Moreover, no visible micro-cracks or structural damage were observed on the material surface or inside the air channels.

This configuration offers notable design advantages. By eliminating external tubing, the embedded channel structure reduces mechanical stress and wear during cyclic operations, significantly enhancing actuator durability while maintaining a compact form factor. The O-ring sealing system ensures leak-proof connections for consistent pneumatic performance over repeated cycles. Furthermore, the modular design facilitates easy maintenance, minimizing downtime during practical deployment.

5.2. Visual perception enabled active grasping

5.2.1. Detection and grasping in single-object scenario

In the experimental setup, each object was placed on the grasping platform multiple times at varying positions to simulate semi-structured scenarios with environmental variability. The grasping process consisted of three sequential steps: target recognition, motion planning, and physical execution. After visual recognition, the target was categorized, and one of the three grasping strategies, namely power grasping, precision grasping, and thumb grasping, was selected. Then, the corresponding pressures for each driving unit were automatically determined, and the grasping process proceeded. For each object, 30 grasping trials were conducted, with detailed records of the detection and grasping outcomes (success/failure) for each attempt (Figure 7(a)). Key performance indicators for successful grasping, including grasping success rate, recognition accuracy, and false detection rate, were calculated (Table II).

Through repeated testing across six distinct object categories, the system exhibited an average visual recognition accuracy exceeding 93%, an average grasping success rate of approximately 87%, and an average operational error rate below 7%. Notably, cylindrical objects demonstrated higher recognition and grasping reliability, whereas spherical and bowl-shaped items were prone to operational deviations, frequently resulting in slippage or failed grasps. This performance discrepancy primarily stems from two factors. First, the structured-light depth camera exhibited sensitivity to ambient lighting, particularly when acquiring depth data from transparent or reflective surfaces, leading to measurement inaccuracies. Second, the dexterous hand's current design shows inferior adaptability to curvilinear geometries, as its

https://doi.org/10.1017/S0263574726103907 Published online by Cambridge University Press

Table II. *Results of detection and grasping in a single-object scenario.*

Object	Number of successful detections	Number of successful grasping	Ratio of successful detections (%)	Ratio of successful grasping (%)	Ratio of grasping failure (%)
Plastic bottle	30	30	100.00	100.00	0.00
Apple	30	25	100.00	83.33	16.67
Plastic bowl	26	26	86.67	86.67	0.00
Orange	30	27	100.00	90.00	10.00
Shuttlecock	27	24	90.00	80.00	11.11
Tennis ball	26	25	86.67	83.33	3.85
Average	28	26	93.89	87.22	6.94

finger kinematics and compliance struggle to maintain stable contact pressure distribution on highly curved objects.

5.2.2. Detection and grasping in multi-object scenario

The experimental evaluation employed a randomized distribution of three object categories with distinct geometric properties across the workspace to replicate dynamic conditions typical of robotic sorting tasks. The robotic system was tasked with autonomously performing three principal functions: scanning and identification of object spatial coordinates, optimal grasp sequence planning, and sequential object transfer execution. A total of 30 trials were performed in this multi-object manipulation scenario, with Figure 7(b) depicting a complete execution cycle of the perception-grasping workflow. Each trial commenced with the robotic arm initialized at a predefined home position, where a 3D camera acquired real-time workspace scans to generate depth-enhanced panoramic representations.

The system first normalized the captured images to standardized dimensions. It then applied a recognition algorithm to detect graspable targets and extract their spatial coordinates. Upon detecting multiple targets, a confidence-based prioritization mechanism selected the highest-scoring recognition instance for initial manipulation. Following each grasping operation, the robotic arm automatically reverted to the home position for workspace re-scanning and state updating, with this closed-loop procedure iterating until complete workspace clearance was achieved.

The system achieved an 83% overall success rate (25 successful grasping in 30 trials) in multi-object grasping scenarios. Although the system initiated motion promptly upon target confirmation, three key factors limited its performance: orientation-dependent pose estimation, actuation timing, and sensitivity to environmental illumination. These findings highlight fundamental challenges in unstructured environments where cumulative perception uncertainties and dynamic physical interactions substantially affect operational reliability. The quantitative outcomes establish valuable benchmarks for enhancing visual recognition robustness and developing adaptive grasping strategies to improve performance in complex manipulation tasks.

6. Conclusion

This study proposes a modular hierarchical design framework to address the structural limitations of conventional rigid dexterous hands, including maintenance difficulties, inadequate pneumatic sealing, and lack of modularity. The developed approach incorporates detachable interfaces and optimized built-in pneumatic channels, enabling both rapid actuator replacement and enhanced air-tightness performance. According to experimental results, the measured maximum fingertip force for fingers is about 2 N at a driving pressure of 300 kPa. The maximum output thrust forces of the thenar and palm actuators were 5.83 N and 10.67 N, respectively. The soft dexterous hand achieved stable load-carrying

https://doi.org/10.1017/S0263574726103907 Published online by Cambridge University Press

capability of 1.97 kg in lifting configuration. The system employs three distinct operational modes: thumb-mediated enveloping, precision pinching for fragile items, and power grasping for heavy loads. Evaluations confirmed that these modes collectively enable versatile manipulation across diverse object sizes, geometries, and textures. A vision-guided manipulation platform was implemented through a hybrid perception method combining RGB imaging with depth data, integrating the dexterous hand, robotic arm, and visual systems into a coordinated framework. This system achieved success rates of 87.22% and 83.33% in single- and multi-object grasping scenarios, respectively, under visual guidance, establishing foundations and providing technical support for engineering implementations of soft robotic manipulators.

Supplementary material. The supplementary material for this article can be found at https://doi.org/10.1017/S0263574726103907.

Author contributions. Ruiqi Yin and Chuanwang Liu conceived and designed the study. Zhenhao Sun and Shihao Sun conducted data gathering. Shuhai Liu and Chuanwang Liu performed statistical analyses. Ruiqi Yin and Huaping Xiao wrote the article.

Financial support. This study was funded by the Beijing Natural Science Foundation (No. 3232013) and the Frontier Interdisciplinary Exploration Research Program of China University of Petroleum, Beijing (No. 2462024XKQY009).

Competing interests. The authors declare no conflicts of interest exist.

Ethical approval. Not applicable.

References

[1] E. A. Alandoli, Y. Fan and D. Liu, "A review of extensible continuum robots: Mechanical structure, actuation methods, stiffness variability, and control methods," *Robotica* **43**(2), 764–791 (2025).
[2] S. Alves, M. Babcinschi, A. Silva, D. Neto, D. Fonseca and P. Neto, "Integrated design fabrication and control of a bioinspired multimaterial soft robotic hand," *Cyborg and Bionic Systems* **4**, 0051 (2023).
[3] B. Calli, A. Singh, A. Walsman, S. Srinivasa, P. Abbeel and A. M. Dollar, "The YCB Object and Model Set: Towards Common Benchmarks for Manipulation Research," **In:** *2015 International Conference on Advanced Robotics (ICAR) 2015* (IEEE, Istanbul, Turkey, 2015) pp. 510–517.
[4] R. Chen, H. Zhang, S. Zhou, X. Xu, Z. Yuan, H. Wang and J. Luo, "A rigid-flexible-soft coupled dexterous hand with sliding tactile perception and feedback," *IEEE Robot. Autom. Lett.* **9**(12), 11682–11689 (2024).
[5] K. Chin, T. Hellebrekers and C. Majidi, "Machine learning for soft robotic sensing and control," *Adv. Intell. Syst.* **2**(6), 1900171 (2020).
[6] A. B. Dawood, J. Fras, F. Aljaber, Y. Mintz, A. Arezzo, H. Godaba and K. Althoefer, "Fusing dexterity and perception for soft robot-assisted minimally invasive surgery: What we learnt from STIFF-FLOP," *Appl. Sci.* **11**(14), 6586 (2021).
[7] R. Deimel and O. Brock, "A novel type of compliant and underactuated robotic hand for dexterous grasping," *Int. J. Robot. Res.* **35**(1–3), 161–185 (2016).
[8] C. Firth, K. Dunn, M. H. Haeusler and Y. Sun, "Anthropomorphic soft robotic end-effector for use with collaborative robots in the construction industry," *Autom. Constr.* **138**, 104218 (2022).
[9] J. Fu, Z. Yu, Q. Guo, L. Zheng and D. Gan, "A variable stiffness robotic gripper based on parallel beam with vision-based force sensing for flexible grasping," *Robotica* **42**(12), 4036–4054 (2024).
[10] J. Guo, F. Guo, H. Zhao, H. Yang, X. Du, F. Fan, W. Liu, Y. Zhang, D. Tu and J. Hao, "In-sensor computing with visual-tactile perception enabled by mechano-optical artificial synapse," *Adv. Mater.* **37**(14), 2419405 (2025).
[11] T. Hao, H. Xiao, Y. Liu, D. Pang and S. Liu, "Gripping performance of soft grippers with fingerprint-like surface texture for objects with slippery surfaces," *Tribol. Int.* **189**, 108992 (2023).
[12] T. Hao, H. Xiao, S. Liu, C. Zhang and H. Ma, "Multijointed pneumatic soft hand with flexible thenar," *Soft Robot.* **9**(4), 745–753 (2022).
[13] D. H. Kim, Y. Lee and H.-S. Park, "Bioinspired high-degrees of freedom soft robotic glove for restoring versatile and comfortable manipulation," *Soft Robot.* **9**(4), 734–744 (2022).
[14] H. Li, C. J. Ford, M. Bianchi, M. G. Catalano, E. Psomopoulou and N. F. Lepora, "BRL/Pisa/IIT softHand: A low-cost, 3D-printed, Underactuated, tendon-driven hand with soft and adaptive synergies," *IEEE Robot. Autom. Lett.* **7**(4), 8745–8751 (2022).
[15] N. Li, Y. Pi, J. Ding and J. Li, Soft hand with programmable grasping mode for dexterous manipulation, 1–16.

https://doi.org/10.1017/S0263574726103907 Published online by Cambridge University Press

[16] H. Liu, C. Wu, S. Lin and Y. Chen, "Finger joint aligned flat tube folding structure for robotic glove design," *Smart Mater. Struct.* **33**(1), 015001 (2024).
[17] X. Liu, Y. Zhao, D. Geng, S. Chen, X. Tan and C. Cao, "Soft humanoid hands with large grasping force enabled by flexible hybrid pneumatic actuators," *Soft Robot.* **8**(2), 175–185 (2021).
[18] Y. Liu, H. Xiao, T. Hao, D. Pang, F. Wang and S. Liu, "Dexterous all-soft hand (DASH) with active palm: Multi-functional soft hand beyond grasping," *Smart Mater. Struct.* **32**(12), 125012 (2023).
[19] M. Otti, D. Monsalve, F. Chapelle, C. Bouzgarrou and Y. Lapusta, "Recent improvements in the development of soft grippers capable of dexterous manipulation," *Appl. Sci.* **15**(1), 275–296 (2024).
[20] M. Pan, C. Yuan, X. Liang, T. Dong, T. Liu, J. Zhang, J. Zou, H. Yang and C. Bowen, "Soft actuators and robotic devices for rehabilitation and assistance," *Adv. Intell. Syst.* **4**(4), 2100140 (2022).
[21] M. Pozzi, M. Malvezzi, D. Prattichizzo and G. Salvietti, "Actuated palms for soft robotic hands: Review and perspectives," *IEEE/ASME Trans. Mechatron.* **29**(2), 902–912 (2024).
[22] S. Puhlmann, J. Harris and O. Brock, "*RBO Hand* 3: A platform for soft dexterous manipulation," *IEEE Trans. Robot.* **38**(6), 3434–3449 (2022).
[23] J. Qu, B. Mao, Z. Li, Y. Xu, K. Zhou, X. Cao, Q. Fan, M. Xu, B. Liang, H. Liu, X. Wang and X. Wang, "Recent progress in advanced tactile sensing technologies for soft grippers," *Adv. Funct. Mater.* **33**(41), 2306249 (2023).
[24] S. Sankar, W.-Y. Cheng, J. Zhang, A. Slepyan, M. M. Iskarous, R. J. Greene, R. DeBrabander, J. Chen, A. Gupta and N. V. Thakor, "A natural biomimetic prosthetic hand with neuromorphic tactile sensing for precise and compliant grasping," *Sci. Adv.* **11**(10), eadr9300 (2025).
[25] H. Wang, F. J. Abu-Dakka, T. Nguyen Le, V. Kyrki and H. Xu, "A novel soft robotic hand design with human-inspired soft palm: Achieving a great diversity of grasps," *IEEE Robot. Autom. Mag.* **28**(2), 37–49 (2021).
[26] Y. Wang, T. Hao, Y. Liu, H. Xiao, S. Liu and H. Zhu, "Anthropomorphic soft hand: Dexterity, sensing, and machine learning," *Actuators* **13**(3), 84 (2024a).
[27] Y. Wang, Z. Xie, H. Huang and X. Liang, "Pioneering healthcare with soft robotic devices: A review," *Smart Med.* **3**(1), e20230045 (2024b).
[28] Y. Yang, Y. Li, Y. Chen, Y. Li, T. Ren and Y. Ren, "Design and automatic fabrication of novel bio-inspired soft smart robotic hands," *IEEE Access* **8**, 155912–155925 (2020).
[29] N. Zhang, L. Ge, H. Xu, X. Zhu and G. Gu, "3D printed, modularized rigid-flexible integrated soft finger actuators for anthropomorphic hands," *Sens. Actuators A: Phys.* **312**, 112090 (2020).
[30] N. Zhang, J. Ren, Y. Dong, X. Yang, R. Bian, J. Li, G. Gu and X. Zhu, "Soft robotic hand with tactile palm-finger coordination," *Nat. Commun.* **16**(1), 2395 (2025).
[31] S. Zhang, Y. Yang, J. Shan, F. Sun, H. Xue and B. Fang, "PaLmTac: A vision-based tactile sensor leveraging distributed-modality design and modal-matching recognition for soft hand perception," *IEEE J. Sel. Top. Signal Process.* **18**(3), 288–298 (2024).
[32] H. Zhou, C. Tawk and G. Alici, "3D printed soft robotic hand with embedded soft sensors for direct transition between hand gestures and improved grasping quality and diversity," *IEEE Trans. Neural Syst. Rehabil. Eng.* **30**, 550–558 (2022).
[33] X. Zhou, G. Chen, B. Jin, H. Feng, Z. Chen, M. Fang, B. Yang, R. Xiao, T. Xie and N. Zheng, "Multimodal autonomous locomotion of liquid crystal elastomer soft robot," *Adv. Sci.* **11**(23), 2402358 (2024).

Cite this article: R. Yin, C. Liu, Z. Sun, S. Sun, S. Liu and H. Xiao (2026). "Soft dexterous hand with enhanced grasping performance enabled by rigid-flexible structure and visual perception", Robotica **44**, 2234–2246. https://doi.org/10.1017/S0263574726103907

https://doi.org/10.1017/S0263574726103907 Published online by Cambridge University Press